crystals

MDPI

Article

Facile Green Synthesis of Zinc Oxide Nanoparticles with Potential Synergistic Activity with Common Antifungal Agents against Multidrug-Resistant Candidal Strains

Mohamed Taha Yassin *, Ashraf Abdel-Fattah Mostafa, Abdulaziz Abdulrahman Al-Askar and Fatimah O. Al-Otibi

Botany and Microbiology Department, College of Science, King Saud University, Riyadh 11451, Saudi Arabia; asali@ksu.edu.sa (A.A.-F.M.); aalaskara@ksu.edu.sa (A.A.A.-A.); falotibi@ksu.edu.sa (F.O.A.-O.)
* Correspondence: myassin2.c@ksu.edu.sa

Abstract: The high incidence of fungal resistance to antifungal drugs represents a global concern, contributing to high levels of morbidity and mortality, especially among immunocompromised patients. Moreover, conventional antifungal medications have poor therapeutic outcomes, as well as possible toxicities resulting from long-term administration. Accordingly, the aim of the present study was to investigate the antifungal effectiveness of biogenic zinc oxide nanoparticles (ZnO NPs) against multidrug-resistant candidal strains. Biogenic ZnO NPs were characterized using physicochemical methods, such as UV-vis spectroscopy, transmission electron microscopy (TEM), energy-dispersive X ray (EDX) spectroscopy, FTIR (Fourier transform infrared) spectroscopy and X-ray powder diffraction (XRD) analysis. UV spectral analysis revealed the formation of two absorption peaks at 367 and 506 nm, which preliminarily indicated the successful synthesis of ZnO NPs, whereas TEM analysis showed that ZnO NPs exhibited an average particle size of 22.84 nm. The EDX spectrum confirmed the successful synthesis of ZnO nanoparticles free of impurities. The FTIR spectrum of the biosynthesized ZnO NPs showed different absorption peaks at 3427.99, 1707.86, 1621.50, 1424.16, 1325.22, 1224.67, 1178.22, 1067.69, 861.22, 752.97 and 574.11 cm^{-1}, corresponding to various functional groups. The average zeta potential value of the ZnO NPs was −7.45 mV. XRD analysis revealed the presence of six diffraction peaks at 2θ = 31.94, 34.66, 36.42, 56.42, 69.54 and 76.94°. The biogenic ZnO NPs (100 µg/disk) exhibited potent antifungal activity against *C. albicans*, *C. glabrata* and *C. tropicalis* strains, with suppressive zone diameters of 24.18 ± 0.32, 20.17 ± 0.56 and 26.35 ± 0.16 mm, respectively. The minimal inhibitory concentration (MIC) of ZnO NPs against *C. tropicalis* strain was found to be 10 µg/mL, whereas the minimal fungicidal concentration (MFC) was found to be 20 µg/mL. Moreover, ZnO NPs revealed a potential synergistic efficiency with fluconazole, nystatin and clotrimazole antifungal drugs against *C. albicans* strain, whereas terbinafine, nystatin and itraconazole antifungal drugs showed a potential synergism with ZnO NPs against *C. glabrata* as a multidrug-resistant strain. In conclusion, pomegranate peel extract mediated green synthesis of ZnO NPs with potential physicochemical features and antimicrobial activity. The biosynthesized ZnO NPs could be utilized for formulation of novel drug combinations to boost the antifungal efficiency of commonly used antifungal agents.

Keywords: green synthesis; pomegranate; nanotechnology; zinc oxide nanoparticles; antifungal; synergism

check for updates

Citation: Yassin, M.T.; Mostafa, A.A.-F.; Al-Askar, A.A.; Al-Otibi, F.O. Facile Green Synthesis of Zinc Oxide Nanoparticles with Potential Synergistic Activity with Common Antifungal Agents against Multidrug-Resistant Candidal Strains. *Crystals* **2022**, *12*, 774. https://doi.org/10.3390/cryst12060774

Academic Editor: Witold Łojkowski

Received: 5 May 2022
Accepted: 25 May 2022
Published: 26 May 2022

1. Introduction

The high incidence of candidal infections results in increased morbidity and death in the human population, especially among severely immunocompromised individuals and those who have spent a lengthy amount of time in hospitals, causing serious nosocomial infections [1]. These infections range from superficial infections that are easily treated

to invasive, life-threatening infections that. Overuse of broad-spectrum antibiotics has exacerbated the situation by resulting in the growth of less sensitive *Candida* strains, particularly non-albicans strains [2]. Despite significant advances in diagnostic and therapeutic techniques, these infections remain a serious problem in intensive care units around the world [3]. *Candida albicans* is the most prevalent candidal pathogen causing bloodstream infections [4]. Moreover, *C. albicans* is a highly adaptable microbe that can acquire resistance to antifungals after extended exposure [5]. *Candida glabrata* is considered the second etiological agent of invasive and mucosal candidiasis, and it was reported as a multidrug-resistant candidal strain [6].

Nanotechnology is a rapidly developing field that deals with the synthesis and characterization of novel nanoscale materials with diameters in the range of 1–100 nm, which have been used in various applications, including biomedical science, health care, food and feed, chemical industries, cosmetics, drug and gene delivery, energy science and electronics [7].

There are several types of nanoparticles, including inorganic, organic and carbon-based nanomaterials [8]. Inorganic nanoparticles include metal and metal-oxide-based nanomaterials that can be synthesized using constructive or destructive methods [9]. The most common metals used in the synthesis of nanomaterials are iron (Fe), zinc (Zn), silver (Ag), aluminum (Al), cadmium (Cd), copper (Cu), cobalt (Co), gold (Au) and lead (Pb) [10]. Metal oxide nanoparticles are used to improve the characteristics of metal nanomaterials. The fundamental goal of metal oxide nanoparticle development is to enhance the reactivity and efficacy of nanoparticles [11]. In this regard, iron oxide (Fe_2O_3), zinc oxide (ZnO), aluminum oxide (Al_2O_3), cerium oxide (CeO_2), magnetite (Fe_3O_4), silicon dioxide (SiO_2) and titanium oxide (TiO_2) are the most commonly fabricated metal oxides [12]. Zinc oxide nanoparticles have recently attracted considerable attention due to their potential use in a wide range of applications, including environmental cleanup, antioxidant activity, biosensors, targeted drug delivery, and agronomic and medicinal applications [13–15]. Microwave-aided synthesis, ultrasonic-assisted synthesis and biological synthesis methods have all been reported as potential ecofriendly techniques for ZnONP synthesis [16]. The use of biological approaches, such as the use of plant extracts or microbes for green production of ZnONPs, has been found to have various advantages over chemical synthesis methods [17]. Green techniques for ZnONP synthesis have several advantages over chemical procedures, including lower toxicity of nanoparticles generated using green methods compared to those synthesized utilizing physicochemical methods [18]. Surface modification of the biosynthesized zinc oxide nanoparticles by the biomolecules utilized in the synthesis process is another advantage of green techniques, acting as a capping and stabilizing agent of the nanomaterials, making them more appropriate and biocompatible in living systems [19]. The main advantages of green synthesis approaches utilizing plant extracts are feasibility, cost effectiveness, ecofriendliness, safety, biocompatibility, high productivity and the considerable variety of ZnO-NPs morphologies depending on the plant extract used, as well as the use of widely available plants for their synthesis [20]. The presence of high amounts of phytochemical compounds in plant extracts has been linked to their potential efficacy in the synthesis of ZnO NPs [21]. Different phytochemical compounds, such as tannins, terpenoids, phenolic compounds, methylxanthines, saponins and alkaloids, were reported as excellent zinc precursor reducers [22]. A mechanistic pathway was reported in several previous studies based on the phytochemical components of the utilized plant extract for the successful syntheis of ZnO NPs [23,24]. These studies demonstrated that plant extracts reduce zinc (II) ions to metallic zinc rather than forming a co-ordinated complex. In [25], after the zinc precursor was completely reduced, a reaction occurred between metallic zinc and dissolved oxygen in the solution, resulting in the production of ZnO nanoparticles. Several previous studies reported the remarkable antimycotic and antibacterial activity of green-synthesized ZnO nanoparticles against different microbial pathogens [26–30]. In this context, aqueous stem extract of *Rutagraveolen* mediated green synthesis of zinc oxide nanoparticles with potential antioxidant and antimicrobial activities [31]. Furthermore, *Passiflora caerulea* fresh leaf extract facilitated green synthesis of

ZnO nanoparticles with remarkable antimicrobial bioactivity against pathogenic microbes causing urinary tract infection [32].

Punica granatum L. (pomegranate) fruit belongs to the Punicaceae family and is eminent based on its phytochemical constituents of phenolic acids, tannins and flavonoids, which have significant nutritional properties [33]. Pomegranate-pericarp aqueous extract functionalized green synthesis of ZnO nanoparticles with potential antibacterial potency against *Bacillus licheniformis*, *Bacillus cereus* and *Escherichia coli* strains [34]. Furthermore, the antibacterial effectiveness of ZnO NPs synthesized using pomegranate extracts was reported against several bacterial pathogens, such as *Klebsiella pneumoniae*, *Staphylococcus aureus*, *Salmonella typhi*, *Bacillus cereus*, *Pseudomonas aeruginosa*, *Streptococcus pneumoniae* and *Aeromonas hydrophila* [35]. In addition, pomegranate peel and coffee ground aqueous extracts are potential reducing agents for green synthesis of ZnONPs, with remarkable antibaterial potency against *P. aeruginosa, S. aureus*, *K. pneumoniae* and *Enterobacter aerogenes* strains [36]. Due to the high prevalence of candidal resistance to routinely used antifungal medicines, new antifungal combinations are needed for effective antifungal therapy and to boost the antifungal activity of common antifungal drugs. Previous reports of ZnO NPs synthesis using *Punica granatum* aqueous extracts focused on the antibacterial efficiency of these nanomaterials against bacteria; pathogens, but no reports have considered their anticandidal efficacy. Furthermore, few studies have investigated the synergistic action of biosynthesized ZnO nanoparticles with routinely used antifungal drugs against multidrug-resistant strains, such as *Candida glabrata* pathogen. Accordingly, the aim of the present study was to investigate the biosynthesis of ZnO nanoparticles using *Punica granatum* aqueous peel extract, characterize these nanomaterials using various physicochemical techniques and evaluate their antifungal effectiveness against multidrug-resistant fungal pathogens. The synergistic antifungal efficiency of these nanomaterials in combination with standard antifungal agents, such as fluconazole, itraconazole, clotrimazole, terbinafine and nystatin, was also investigated.

2. Materials and Methods

2.1. Preparation of Pomegranate Peel Extract

Pomegranate fruits were purchased from a local market in Riyadh, Saudi Arabia. The pomegranate peels were rinsed twice with tap water before being washed with distilled water. After complete drying, the pomegranate peels were pulverized into a homogeneous powder using a mechanical mortar. Fifty grams of the powdered plant materials was submerged in 500 mL flasks containing 200 mL of deionized water and heated over a hot plate for at 50 °C for 30 min. The flasks were then incubated at 25 °C for 24 h under magnetic stirring; then, the extracts were filtered using Whatman grade 1 filter paper. The plant extracts were stored in a refrigerator at 4 °C for further use [37].

2.2. Synthesis of Zinc Oxide Nanoparticles

Zinc nitrate hexahydrate ($Zn(NO_3)_2 .6H_2O$) of reagent grade (98%) was purchased from Sigma-Aldrich, Poole, Dorset, U.K. A total of 0.01 M zinc nitrate hexahydrate ($Zn(NO_3)_2 .6H_2O$) solution was used for green synthesis of zinc oxide nanoparticles using the prepared aqueous pomegranate peel extract. Briefly, 5 mL of plant extract was added to 95 mL of zinc nitrate solution (0.01 M) in 250 mL flasks. The flasks were incubated over a magnetic stirrer (150 rpm) at 70 °C for 1 h. Change of color and formation of bioreduced precipitates indicated the formation of zinc oxide nanoparticles. The reduced precipitates were collected by centrifugation at 10,000 rpm for 10 min. After centrifugation, supernatants were discarded, and the formed precipitates were washed thrice with distilled water to remove impurities [38,39].

2.3. UV-Vis Spectroscopy

The biogenic ZnO NPs were initially dispersed in distilled H_2O, and then the optical diffuse reflectance was measured in a wavelength range of 200–800 nm using a UV–VIS-NIR spectrophotometer (UV-1601, Shimadzu, Kyoto, Japan).

2.4. Transmission Electron Microscopy (TEM) Analysis

The biogenic ZnO NPs were rinsed three times with deionized water. Before testing, the samples were placed on a carbon-coated copper grid, detached and finally dried before examination. The examination was conducted using a transmission electron microscope (JEOL, JEM1011, Tokyo, Japan) at the Electron Microscope Unit of the College of Science at King Saud University. TEM was used to investigate the morphological features through generation of high-resolution two-dimensional images at a voltage of 100 kV. A particle size distribution histogram was plotted to detect the average particle size of the biosynthesized ZnO NPs.

2.5. Energy-Dispersive X-ray (EDX) Analysis

Elemental mapping of the biosynthesized ZnO NPs was performed using a scanning electron microscope (SEM) equipped with an energy-dispersive X-ray (EDX) analyzer (JEOL, JSM-6380 LA, Tokyo, Japan).

2.6. FTIR (Fourier Transform Infrared) Analysis

Fourier transform infrared spectroscopy (Shimadzu, Kyoto, IR Affinity 1, Japan) was used for determination of the functional groups of the synthesized ZnO nanoparticles. Depending on the infrared absorption frequency, the functional groups bound to the nanoparticle surface were detected in the range of 400–4000 cm^{-1}. The samples were prepared by dispersing the zinc oxide nanomaterials in a dry KBr matrix and compacting the disc to form a transparent sample. A KBr pellet was used as control, [40].

2.7. X-ray Powder Diffraction (XRD) Analysis

A Shimadzu XRD model 6000 diffractometer (Shimadzu, Columbia, MD, USA) equipped with a graphite monochromator was used to analyze X-ray powder diffraction (XRD) patterns with Cu-K radiation. The XRD pattern was measured on a film of biosynthesized ZnO NPs using step-scanning software with a resolution of 0.02 per step and an acquisition time of 5 s per step at 2 theta. The crystalline phases were identified according to ICDD (International Center for Diffraction Data) standards.

2.8. Screening of Antifungal Activity of the Biosynthesized ZnO Nanomaterials

Three candidal strains, namely, *C. albicans* (ATCC 29213), *C. tropicalis* (ATCC 33592) and *C. glabrata* (ATCC 25922), were assayed for their susceptibility to the biosynthesized ZnO NPs. The antifungal efficiency of the biosynthesized ZnO NPs was screened using a standard disk diffusion method against the concerned candidal pathogens [41]. The candidal suspension was prepared using 0.9% NaCl solution, and the microbial turbidity was adjusted using 0.5 McFarland standard. Mueller–Hinton agar (MHA) medium supplemented with 0.5 μg/mL methylene blue and 2% glucose was prepared and poured into sterile Petri dishes. Finally, the prepared microbial suspension was streaked over the poured MHA plates using sterile swabs. The dried ZnO nanoparticles were suspended in methanol solvent; then, sterile filter paper disks (8 mm in diameter) were impregnated with the dissolved ZnO nanomaterials to attain final concentrations of 50 and 100 μg/disk. Terbinafine disks (30 μg/disk) as standard antifungal agents were used as positive controls, whereas negative controls were filter paper disks impregnated with methanol solvent only. The suppressive zones were measured using a vernier caliper after the plates were incubated at 35 °C for 24 h. Minimum inhibitory concentration (MIC) was determined using a broth microdilution assay, as recommended in CLSI document M27-Ed4, to detect the lowest concentration of ZnO NPs exhibiting anticandidal efficiency [42]. The

minimum fungicidal concentration (MFC) was determined by streaking inoculums from MIC wells into freshly prepared MHA plates and checking for fungal growth. The lowest concentration of ZnO NPs resulted in no bacterial growth and was registered as MFC [43].

2.9. Detection of Synergistic Activity of the Biosynthesized ZnO NPs with Antifungal Drugs

The synergistic efficiency of the biogenic ZnO NPs in combination with commonly used antifungal agents against the tested fungal pathogens was detected using the standard disk diffusion method [41,44–46]. Sterile filter paper disks were impregnated with 10 µg, 25 µg, 20 µg, 30 µg and 10 µg of itraconazole, fluconazole, nystatin, terbinafine and clotrimazole as standard antifungal agents, respectively, whereas another group of filter paper disks was loaded with the same concentrations of antifungal drugs plus the MIC of the biogenic ZnONPs. In addition, filter paper disks impregnated with methanol solvent only were used as negative controls. Finally, filter paper disks loaded with ZnO NPs (10 µg/disk) were prepared to compare the anticandidal effectiveness with that of other groups. Seeded MHA plates were prepared as mentioned above, and the loaded filter paper disks were placed over the seeded plates. The plates were incubated at 25 °C for 24 h after being preserved for 2 h in a refrigerator to allow for ZnO NPs diffusion. Finally, the plates were checked for the formation of inhibition zones, and the zone diameters were measured using a vernier caliper. Synergistic efficiency was determined by the equation $\frac{B-A}{A} \times 100$, where A and B are the inhibition zone diameters for antifungal and antifungal + ZnO NPs, respectively [47].

2.10. Statistical Analysis

The anticandidal activity data of the biogenic ZnO NPs were statistically analyzed using GraphPad Prism 5.0 (GraphPad Software, Inc., La Jolla, CA, USA) with one-way analysis of variance and Tukey's test. The data are presented as mean of triplicates ± standard error. A particle size distribution histogram and XRD pattern were plotted using OriginPro 2018.

3. Results and Discussion

3.1. Synthesis of Zinc Oxide Nanoparticles

Figure 1A depicts *Punica granatum* aqueous peel extract, whereas Figure 1B depicts the colorless zinc nitrate solution. Synthesis of ZnO NPs was preliminarily confirmed by visual observation of dark-yellow precipitate, as seen in Figure 1C. Pomegranate peel extract was previously reported to be rich in phytochemical components, which act as reducing and stabilizing agents for the successful synthesis of zinc oxide nanoparticles [12]. In this regard, the main phytochemical ingredients of pomegranate peel extract were found to be punicalagin, gallic acid, ellagic acid, caffeic acid, cinnamic acid, p-coumaric acid and chlorogenic acid, as demonstrated in previous reports [17,48]. The mechanism of zinc oxide nanoparticle formation was reported in a prior study, where it was shown that the phytochemical compounds denoted their electrons and contributed to the stabilization of positively charged Zn^{2+} ions; then, thermal annealing was performed for the conversion of Zn^{2+} complex ions to ZnO nanoparticles [49].

3.2. UV-Vis Spectral Analysis

UV-vis spectra of the synthesized zinc oxide nanoparticles indicated the presence of two distinctive adsorption peaks at 367 and 506 nm. The biosynthesis of ZnO nanoparticles using a green synthesis approach was demonstrated by the characteristic peaks identified at 367 and 506 nm, which indicated the surface plasmon resonance of the biogenic ZnO NPs (Figure 2). Our findings are consistent with those of a previous study, which showed the formation of ZnO nanoparticles at wavelengths of 366 and 509 nm [50]. Another study reported that surface plasmon vibrations of biogenic ZnO nanoparticles synthesized using aqueous *Punica granatum* leaf extract caused an absorbance peak at 382 nm, demonstrating the reduction of zinc nitrate hexahydrate into ZnO NPs [51]. The band gap energy of the synthesized ZnO nanoparticles was estimated using Tauc's plot method [52] and

estimated to be 3.4 eV, as seen in Figure 3 [53]. Our findings are in accordance with those of Ramesh et al. (2015), who reported that the indirect band gap energy of biogenic ZnO synthesized using *Solanum nigrum* leaf extract was 3.4 eV [54]. The optical band gap energy of the formulated ZnO NPs in another previous study was estimated using the Tauc plot method, obtaining a value of 3.39 eV [55]. Tauc plots indicated that the band gap energy of zinc oxide nanoparticles (ZnO NPs) and nanosheets (ZnO NSs) were 3.42 eV and 3.23 eV, respectively [56]. Another study confirmed the green sonochemical synthesis of ZnO nanoparticles with a band gap energy of 3.4 eV, which was estimated using the Tauc plot method [57].

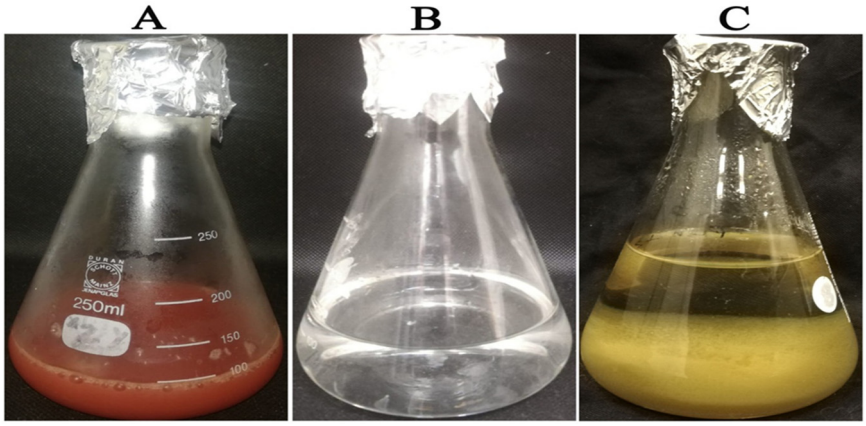

Figure 1. Synthesis of zinc oxide nanoparticles utilizing *Punica granatum* peel extract. (**A**) pomegranate peel aqueous extract; (**B**) colorless zinc nitrate hexahydrate solution; (**C**): dark-yellow precipitate formation indicating synthesis of ZnO NPs.

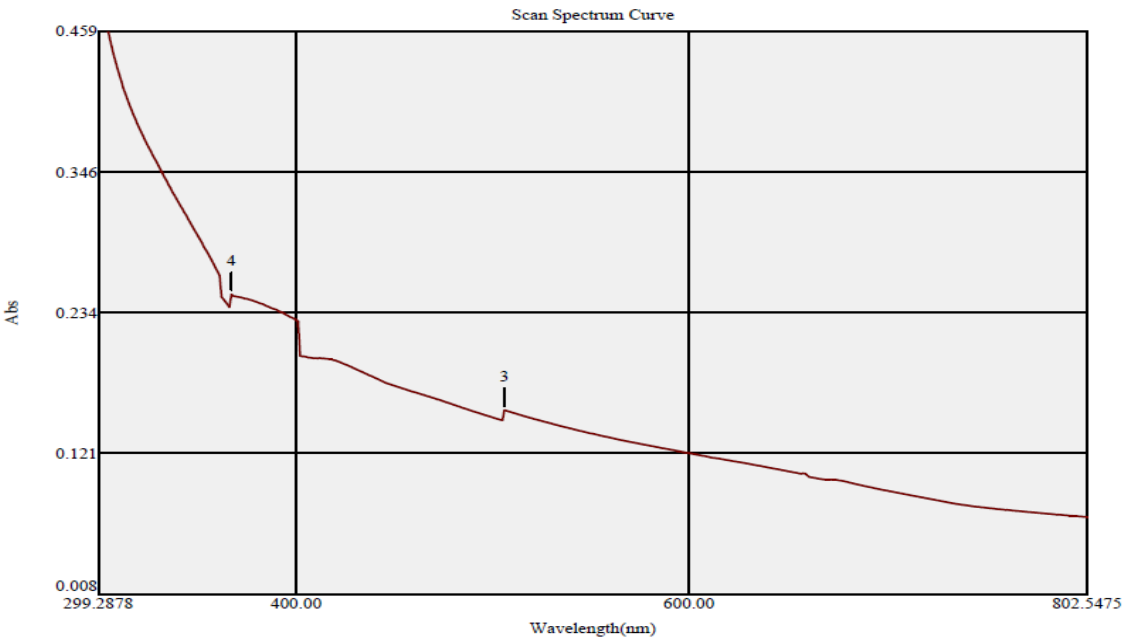

Figure 2. UV-vis spectrum of zinc oxide nanoparticles synthesized using aqueous pomegranate extract (Peak 3: 506 nm; Peak 4: 367 nm).

3.3. Transmission Electron Microscope (TEM) Analysis

Transmission electron microscope (TEM) analysis was performed to determine the morphology and size of the biosynthesized ZnO nanoparticles [37]. TEM micrographs indicated the formation of ZnO nanoparticles ranging in size from 10 to 50 nm, with varied shapes, such as spheres, quasi-spheres, triangles and hexagons, as seen in Figure 4. The particles size distribution indicated that the average particle size diameter of the synthesized

ZnO nanoparticles was 22.84 ± 1.12 nm (Figure 5). Our results are in agreement with those of Sukri et al. (2019), who confirmed the green synthesis of ZnO nanoparticles utilizing pomegranate peel extracts with spherical and hexagonal shapes with an average particle size diameter of 32.98 nm [49]. Moreover, TEM micrographs showed the core-shell structure of the biosynthesized ZnO nanoparticles, owing to the immobilization of the biomolecules of pomegranate peel extract on the nanoparticle surface during the synthesis process [58].

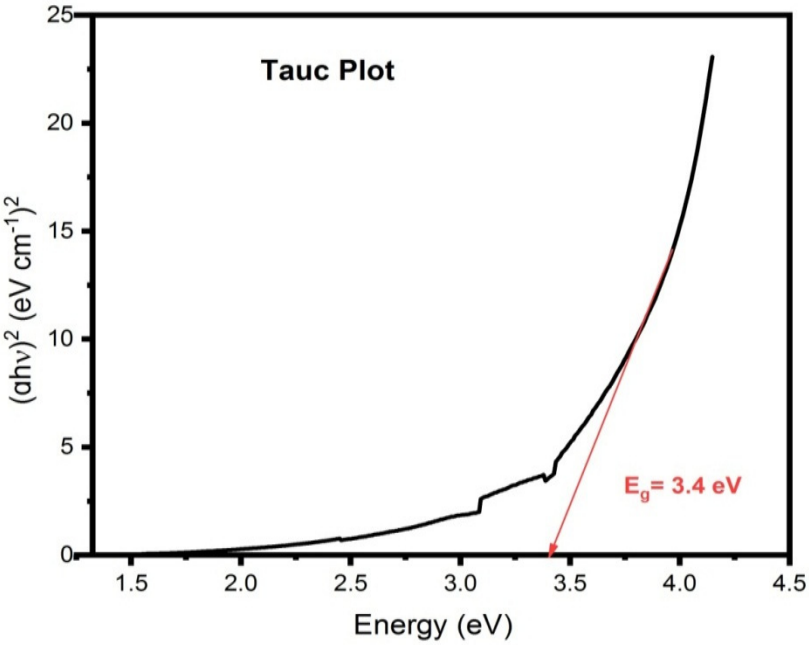

Figure 3. Band gap energy of the biosynthesized ZnO nanoparticles using the Tauc plot method.

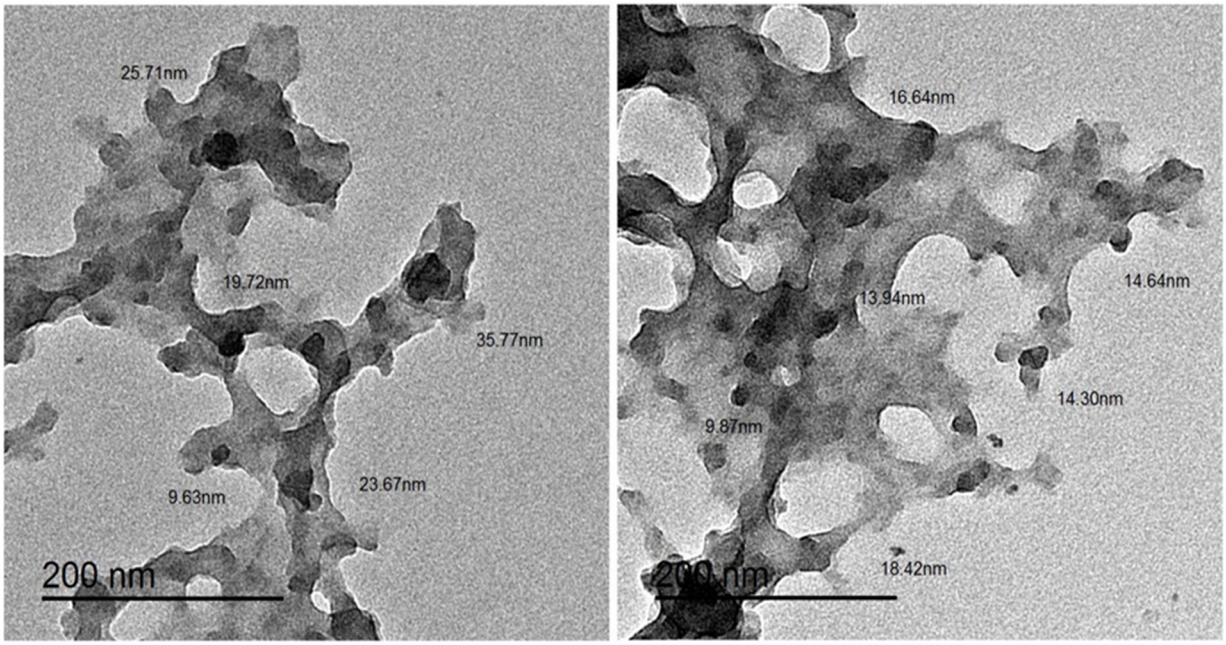

Figure 4. *Cont.*

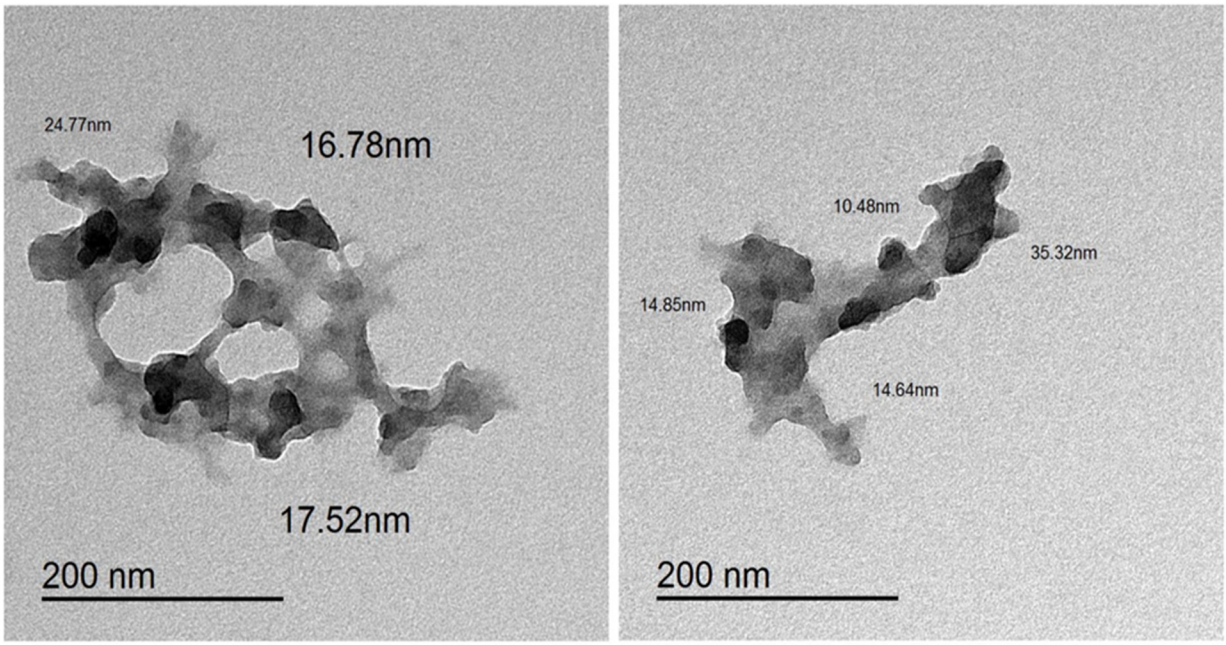

Figure 4. TEM micrographs of zinc oxide nanoparticles synthesized using pomegranate peel extract.

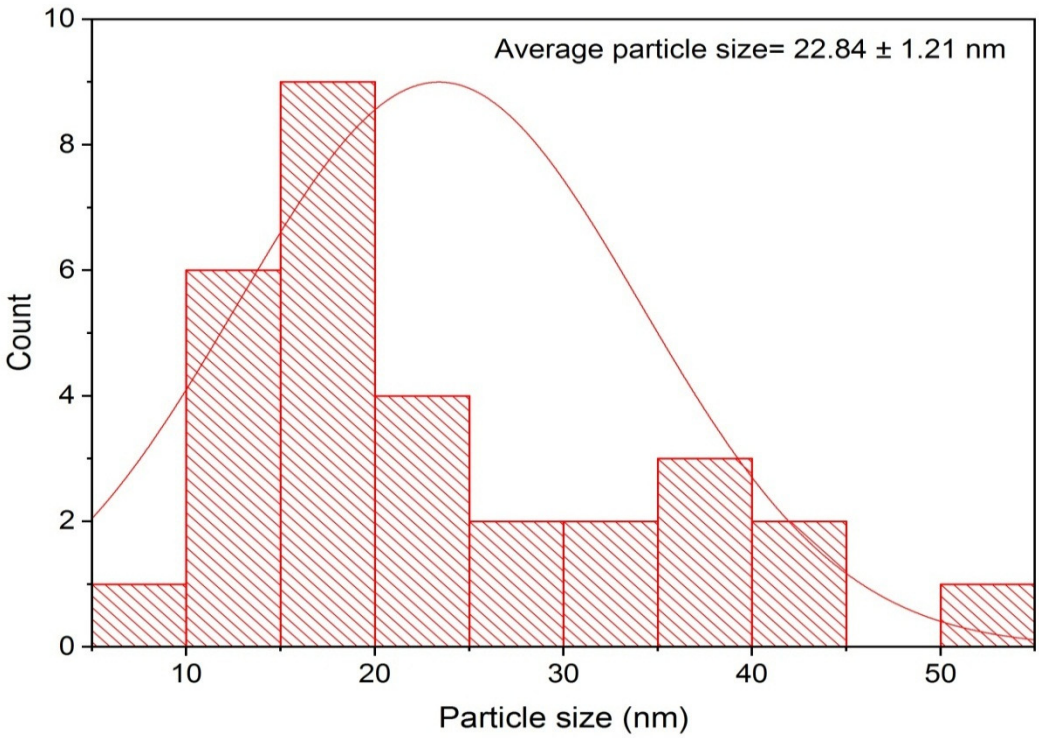

Figure 5. Particle size distribution of zinc oxide nanoparticles synthesized using aqueous pomegranate extract.

3.4. EDX Analysis

Energy-dispersive X-ray (EDX) analysis was performed for the elemental mapping of the green biosynthesized ZnO nanoparticles. The analysis revealed the presence of oxygen and zinc, with corresponding mass percentages of 7.44 and 30.40%, respectively (Figure 6), confirming the formation of zinc oxide nanoparticles. The carbon peak can be attributed to carbon tape used during measurement, as well as the carbon adsorbed on the surface during sample exposure to the ambient atmosphere [59]. The EDX spectrum confirmed the successful synthesis of ZnO nanoparticles free of impurities. The spectrum also revealed

the presence of strong peaks at 0.5, 1.1, 8.6 and 9.5 keV, which were assigned to O *Kα*, Zn *Lα*, Zn *Kα* and Zn *Kβ*, respectively; our findings are in agreement with those reported in a prior study [60].

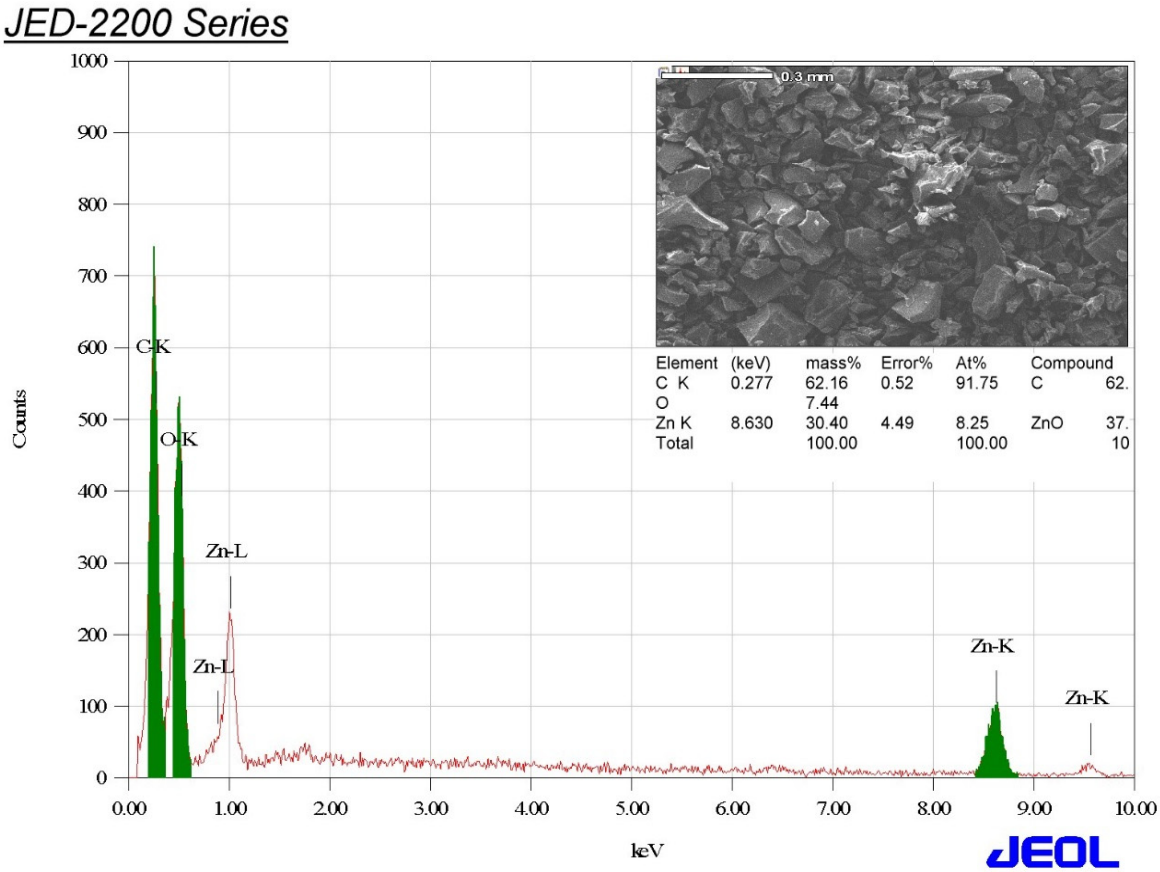

Figure 6. EDX analysis and SEM micrograph of the green synthesized zinc oxide nanoparticles.

3.5. Fourier Transform Infrared Spectroscopy (FTIR) Analysis

FTIR analysis was carried out to detect different functional groups contributing to reduction, capping and stabilization of the biosynthesized ZnO nanoparticles [39]. Different absorption peaks of the biosynthesized ZnO NPs were detected at 3427.99, 1707.86, 1621.50, 1424.16, 1325.22, 1224.67, 1178.22, 1067.69, 861.22, 752.97 and 574.11 cm^{-1}, as seen in Figure 7. The broad absorption band at 3427.99 cm^{-1} assigned to O-H stretching of free hydroxyl groups could be assigned to the polyphenolic compounds of pomegranate peel extract [35]. *Morinda Citrifolia* leaf extract mediated green synthesis of selenium nanoparticles, with an absorption band at 3427.99 cm^{-1} corresponding to the O-H stretching of phenolic compounds of the extract [61]. Another study confirmed the green synthesis of silver nanoparticles utilizing aqueous leaf extract of *Aegle marmelos*, with the formation of an absorption band at 3339 cm^{-1} which can be assigned to O-H stretching of phenolic compounds [62]. Furthermore, the absorption peak at 1707.86 cm^{-1} indicated the C=O stretching of ketones and carboxylic acids, whereas the peak detected at 1621.50 cm^{-1} revealed the C=C stretching of alkenes. On the other hand, the peaks observed at 1424.16 and 1325.22 cm^{-1} demonstrated O-H bending of carboxylic acids and phenolic compounds. The two other successive absorption peaks detected at 1224.67 and 1178.22 cm^{-1} were assigned to C-N stretching of amine functional groups (Table 1). Moreover, the absorption band observed at 1067.69 cm^{-1} corresponded to C-O stretching of alcohols, whereas the weak absorption band at 861.22 cm^{-1} was assigned to C-H bending of aromatic compounds. The absorption bands observed at 752.97 and 574.11 cm^{-1} were assigned to C-Cl and C-Br stretching of alkyl halides, respectively. Overall, the detection of different functional groups within the biogenic ZnO nanoparticles, such as phenols, ketones, carboxylic acids, alkenes,

amines, alcohols and aromatic compounds, may have participated in the reduction of Zn^{2+} and also served as capping and stabilizing agents of the biogenic ZnONPs.

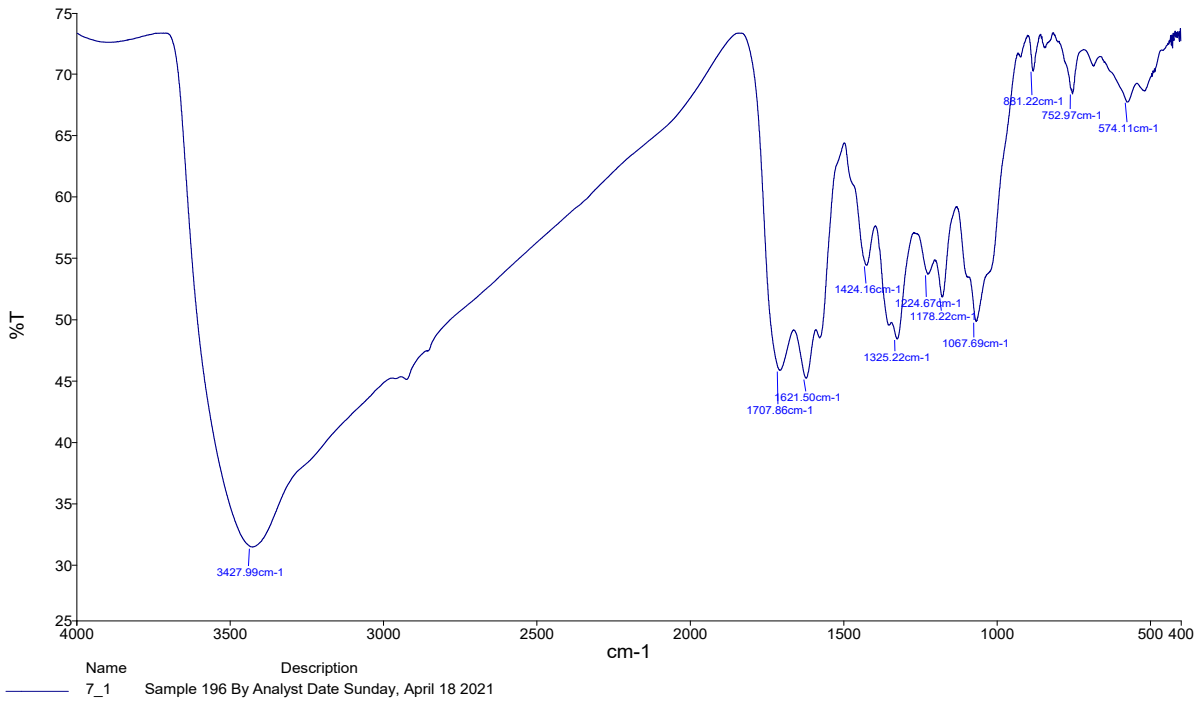

Figure 7. FTIR spectrum of the biogenic ZnO NPs synthesized using pomegranate peel extract.

Table 1. Functional groups of the biogenic ZnO NPs synthesized using aqueous extract of pomegranate peel.

No.	Absorption Peak (cm^{-1})	Appearance	Functional Group	Molecular Motion
1	3427.99	Strong, broad	Phenols	O-H stretching
2	1707.86	Medium	Ketones or carboxylic acids	C=O stretching
3	1621.50	Medium	Alkenes	C=C stretching
4	1424.16	Medium	Carboxylic acids	O-H bending
5	1325.22	Medium	Phenols	O-H bending
6	1224.67	Medium	Amines	C-N stretching
7	1178.22	Medium	Amines	C-N stretching
8	1067.69	Medium	Alcohols	C-O stretching
9	861.22	Weak	Aromatic compounds	C-H bending
10	752.97	Weak	Halo compounds	C-Cl stretching
11	574.11	Weak, broad	Halo compounds	C-Br stretching

3.6. X-ray Diffraction (XRD) Analysis

X-ray diffraction (XRD) analysis showed the presence of six diffraction peaks with 2θ values of 31.94°, 34.66°, 36.42°, 56.42°, 69.54° and 76.94° (Figure 8) corresponding to crystal planes of (100), (002), (101), (110), (112) and (202), respectively, according to the Joint Committee on Powder Diffraction Studies Standards (JCPDS card numbers 008, 82–1042 and 5–0664) [63–65]. In the XRD pattern, the presence of planes (100), (002), (101), (110), (112) and (202) affirmed the formation of a pure wurtzite structure in the ZnO NPs [66]. Similar findings were reported by Ifeanyichukwu et al. (2020) who reported that biogenic ZnO nanoparticles synthesized using pomegranate flower extract revealed seven diffraction peaks at 2θ values of 36.25°, 47.54°, 56.62°, 62.76°, 68.00°, 69.10° and 72.43°, corresponding to lattice planes of (100), (002), (101), (102), (110), (103), (200), (112), (201) and (202), respectively [30]. The narrow and sharp peaks of the XRD pattern affirmed the fine crystalline structure of the biosynthesized zinc oxide nanoparticles [67].

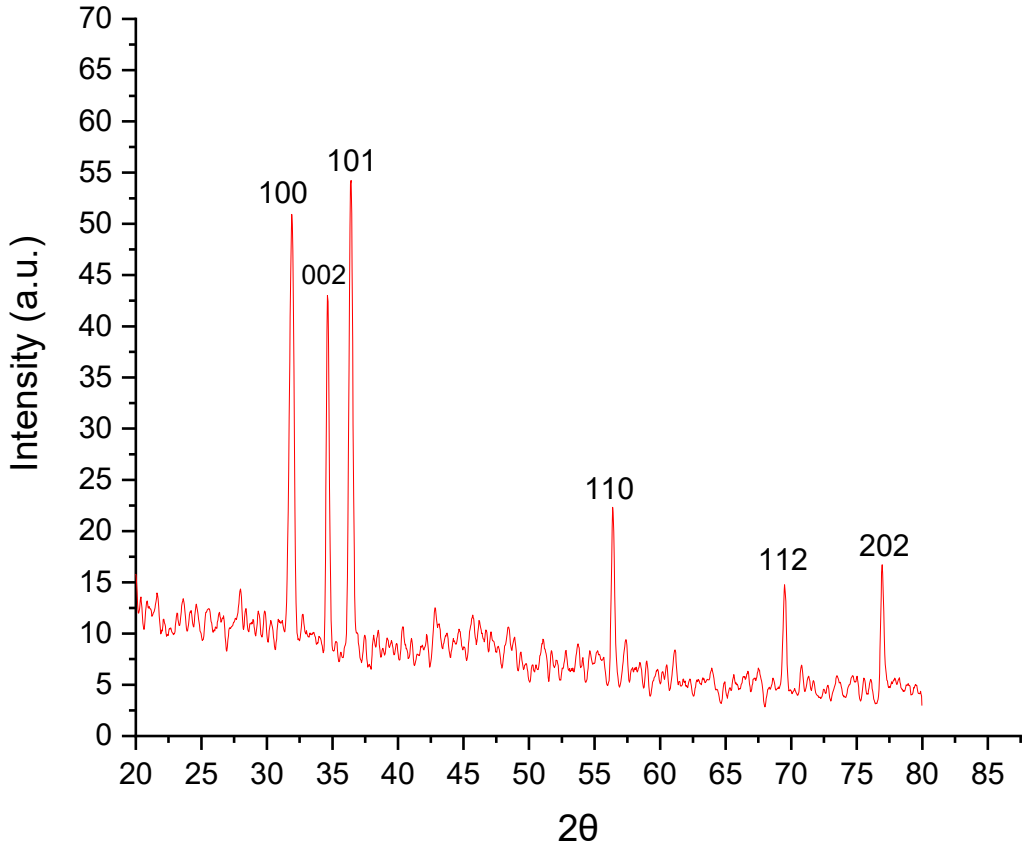

Figure 8. XRD analysis of zinc oxide nanoparticles synthesized using aqueous pomegranate peel extract.

3.7. Zeta Potential Analysis of the Biogenic ZnONPs

Dynamic light scattering (DLS) and zeta potential analysis of the biogenic ZnO NPs were performed to determine the average particle size and charge of the biosynthesized ZnO NPs [68]. The average particle size, as calculated by DLS, was found to be 46.22 nm, which is higher than that detected by TEM analysis, owing to the polydisperse nature of the synthesized nanoparticles, as indicated by the polydispersity index value of 0.611 (Figure 9A). The accumulation of extra hydrate layers on the nanoparticle surface resulted in the detection larger biogenic ZnO nanoparticles than those detected by TEM analysis [69].

Zeta potential analysis was performed to detect the surface charge of biosynthesized ZnO NPs [70]. The average zeta potential value of the biosynthesized ZnO nanoparticles was found to be −7.45 mV (Figure 9B). This result confirmed that the capping biomolecules present on the biosynthesized ZnO NPs were mostly consisted of negatively charged groups [71]. The detected negative charge of the biogenic ZnO NPs revealed the electrostatic repulsion between the synthesized nanoparticles [72].

3.8. Screening of Anticandidal Efficiency of the Biosynthesized ZnO Nanoparticles

A disc diffusion assay was conducted to assess the antifungal efficiency of the biosynthesized ZnO nanoparticles against the concerned candidal strains [73]. The biogenic ZnO nanoparticles exhibited antifungal efficiency at a concentration of 50µg/disc against *C. glabrata*, *C. albicans* and *C. tropicalis*, with inhibitory zone diameters of 18.68 ± 0.37, 21.36 ± 0.19 and 23.12 ± 0.21 mm, respectively (Table 2). *Candida tropicalis* exhibited the highest susceptibility to the biosynthesized ZnO NPs, whereas *C. glabrata* revealed the lowest susceptibility, with inhibitory zones of 26.35 ± 0.16 and 20.17 ± 0.56 mm, respectively, at a ZnO NP concentration of 100 µg/disc. The antifungal efficiency of the biogenic ZnO NPs (100 µg/disc) against *C. glabrata* was twofold higher than that of the control. A prior study demonstrated the antifungal efficacy of biogenic ZnO NPs (1 mg/mL) synthesized

using aqueous leaf extract of *Girardinia diversifolia* against *C. albicans* with an inhibitory zone diameter of 20.23 ± 0.65 mm [74]. Overall, the antifungal effectiveness of the biogenic ZnO NPs was significantly higher than that reported in a previous study, where the used concentration was 1 mg/mL, which is 20-fold higher than that used in the current study (50 µg/L), with inhibition zone diameters of 20.23 ± 0.65 and 21.36 ± 0.19 mm against *C. albicans* strain.

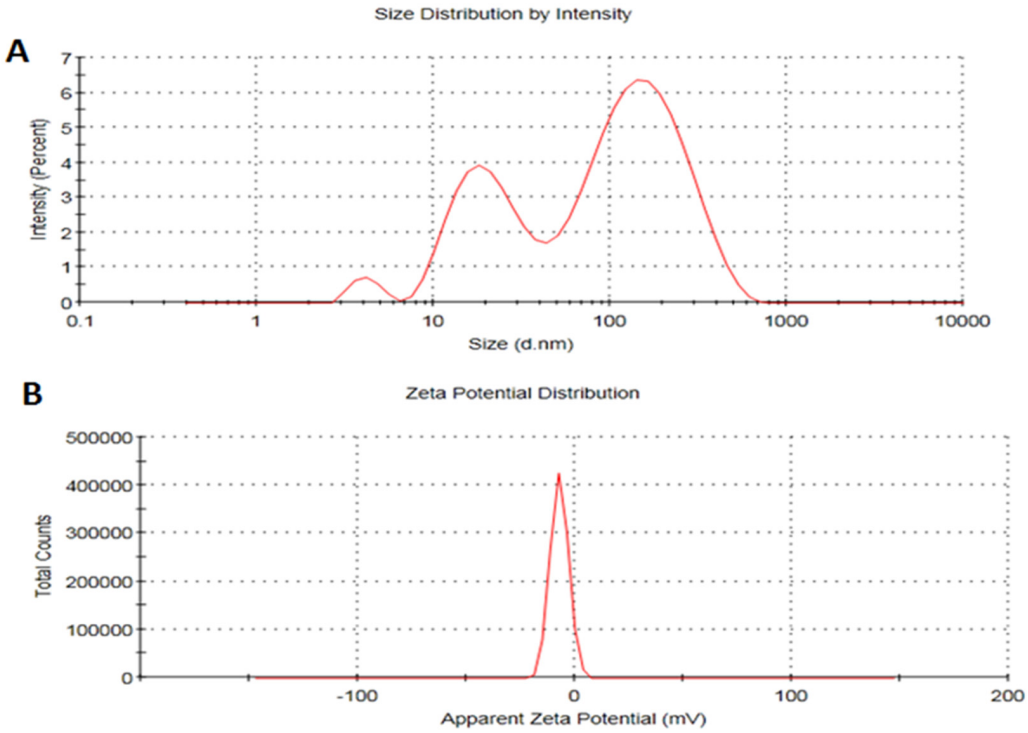

Figure 9. Zeta potential analysis of the biosynthesized ZnO nanoparticles; (**A**) for Size distribution pattern of the biogenic ZnO NPs; (**B**) for Zeta potential analysis of the biosynthesized ZnO NPs.

Table 2. Screening of antifungal efficiency of the biogenic ZnO NPs against the tested strains.

Concentration (µg/Disk)	Inhibition Zone Diameter (mm)		
	C. albicans	*C. glabrata*	*C. tropicalis*
ZnO NPs (50 µg/disk)	21.36 ± 0.19	18.68 ± 0.37	23.12 ± 0.21
ZnO NPs (100 µg/disk)	24.18 ± 0.32	20.17 ± 0.56	26.35 ± 0.16
Terbinafine (30 µg/disk)	27.98 ± 0.11	10.69 ± 0.14	33.81 ± 0.28
negative control	0.00 ± 0.00	0.00 ± 0.00	0.00 ± 0.00

The minimum inhibitory concentration (MIC) of ZnO NPs was tested against *C. tropicalis*, which was found to have the highest susceptibility to the biosynthesized nanoparticles. The MIC of the biogenic ZnO NPs against *C. tropicalis* strain was found to be 10 µg/mL, whereas the minimum fungicidal concentration (MFC) was found to be 20 µg/mL. These findings were significantly higher than those reported in a previous study, which reported that the aqueous extract of the aerial parts of *Prosopis farcta* mediated green synthesis of ZnO nanoparticles, with MIC and MFC values of 128 and 256 µg/mL, respectively [75]. Taken together, the MIC results affirmed the potent antifungal efficiency of the biogenic ZnO NPs against different candidal strains compared to previous studies.

3.9. Synergistic Antifungal Efficiency of the Biogenic ZnO Nanoparticles with Common Antifungal Agents

The antifungal activity of common antifungal agents, such as fluconazole, itraconazole, clotrimazole, terbinafine and nystatin, against different tested strains was evaluated using

the disk diffusion method. Furthermore, the synergistic activity of the biosynthesized ZnO nanomaterials with antifungal agents was investigated.

Candidal infections are commonly treated with such azole antifungal drugs as fluconazole, itraconazole and clotrimazole [76]. The antifungal activity of azoles against *Candida* strains is mediated by the disruption of lanosterol 14-α-sterol demethylase, which is involved in the biosynthesis of ergosterol [77]. Inhibition of lanosterol 14-α-sterol demethylases results in disruption of candidal growth by disturbing the fungal cell membrane [78].

Antifungal susceptibility testing revealed the resistance of *C. glabrata* to itraconazole, nystatin and terbinafine antifungal agents, whereas *C. albicans* exhibited resistance to fluconazole (Figure 10). Similar findings were reported in a prior study, which revealed that isolated clinical strains of *C. albicans* and *C. glabrata* were resistant to fluconazole and itraconazole, respectively [79]. Furthermore, Lakshmy et al. (2016) demonstrated fluconazole resistance in 6% of isolated *C. albicans* strains [80]. In this regard, the candidal resistance to azoles involves the expression of multidrug efflux pumps in the fungal cell wall and alteration of the *ERG11* gene encoding for lanosterol 14-α-sterol demethylase [81].

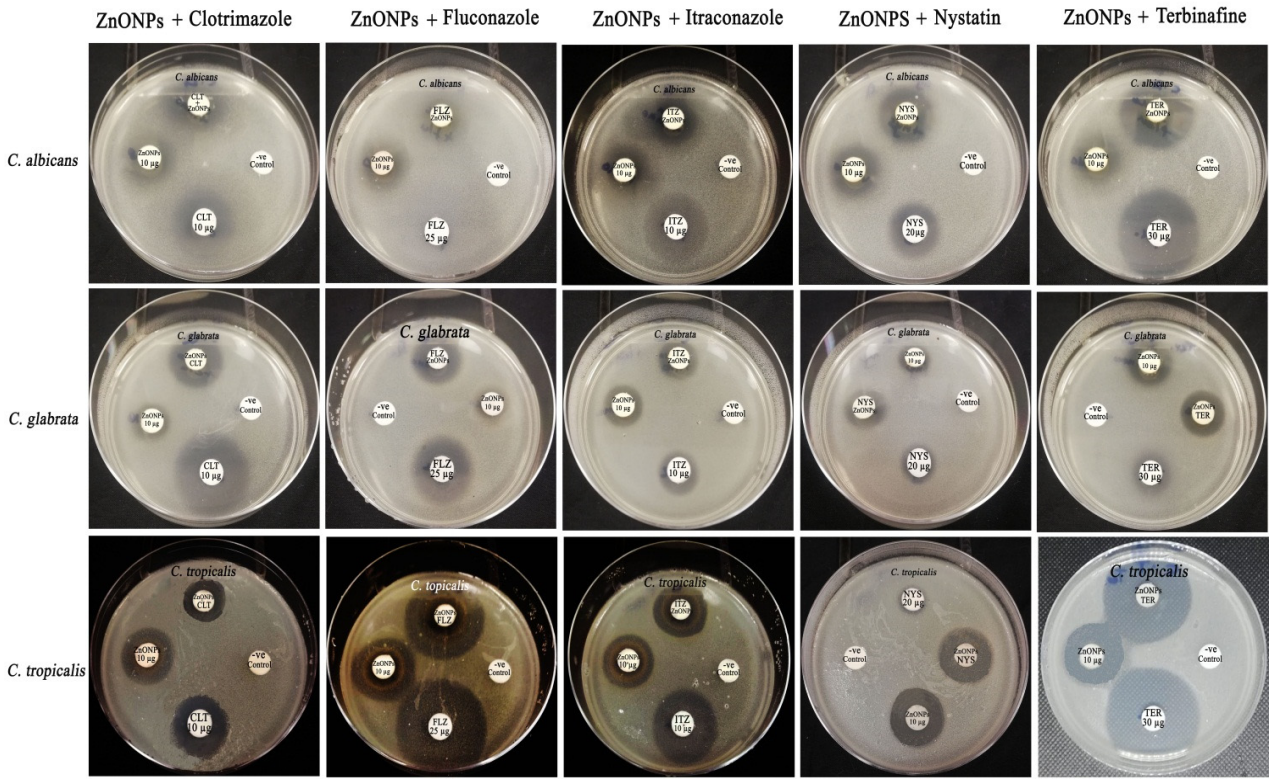

Figure 10. Synergistic antifungal efficiency of the biogenic ZnO NPs with common antifungal agents.

Nystatin is considered one of the most commonly used antifungal drugs, and it is classified as a polyene [82]. The suggested mechanism of antifungal action of nystatin was reported to be the pore-forming action by which nystatin interacts with ergosterol to form ion-leaking pores in the candidal membrane [83]. Both *C. glabrata* and *C. tropicalis* demonstrated resistance to nystatin antifungal agent. Esfahani et al. (2019) reported the resistance of *C. albicans*, *C. glabrata*, *C. kefyr*, *C. stellatoidea* and *C. krusei* strains to nystatin and fluconazole antifungal agents [84]. The resistance mechanism of *Candida* sp. to nystatin was assigned to a decreased binding affinity between nystatin and sterols [85].

Terbinafine belongs to the allylamine class of antifungals, and it undergoes fungicidal action through inhibition of squalene epoxidase (*Erg1p*) in the ergosterol biosynthesis pathway, resulting in increased membrane permeability and initiation of fungal cell death [86]. Only *C. glabrata* was resistant to terbinafine antifungal, whereas *Candida albicans* and *Candida tropicalis* were found to be terbinafine sensitive. Fatahinia et al. (2020) reported that 80% of isolated *C. glabrata* strains were resistant to terbinafine antifungal drugs [87]. The

resistance of candidal strains to terbinafine has been linked to a single missense mutation in the squalene epoxidase gene, resulting in amino acid substitutions [88]. Due to the detected resistance of *Candida* strains, the synergistic effectiveness of biogenic ZnO nanoparticles was evaluated in order to boost the antifungal efficiency of the tested antifungal medications. In this regard, the synergistic activity of the biosynthesized ZnO nanoparticles at MIC (10 µg/mL), in combination with common antifungal agents against different candidal strains, was evaluated using a disk diffusion method. The biogenic ZnO NPs revealed a potential synergistic efficiency with fluconazole, nystatin and clotrimazole antifungal drugs against *C. albicans* strains, with relative synergistic percentages of 92.15, 49.64 and 33.29%, respectively. Furthermore, a potential synergistic action was detected between the biogenic ZnO nanoparticles and terbinafine, nystatin and itraconazole antifungal drugs against the multidrug-resistant strain *C. glabrata*, demonstrating relative synergism percentages of 81.63, 56.40 and 49.95%, respectively (Figure 11). In addition, a significant synergistic antifungal efficiency was detected between ZnO NPs and nystatin, with a relative synergism percentage of 150.38%. Moderate synergistic activities were detected between ZnO NPs and terbinafine against *C. albicans*, whereas a weak synergistic activity was detected between ZnO NPs and itraconazole against *C. tropicalis*, with relative synergism percentages of 14.50 and 5.66%, respectively. On the other hand, antagonistic action was detected between the biosynthesized ZnO NPs and both terbinafine and clotrimazole against *C. tropicalis* (Table 3). Overall, the potential synergistic efficiency of the biogenic ZnO NPs with different antifungal agents against the tested candidal pathogens highlights the potential of utilizing these nanomaterials in formulations of novel antifungal agents against multidrug-resistant candidal pathogens.

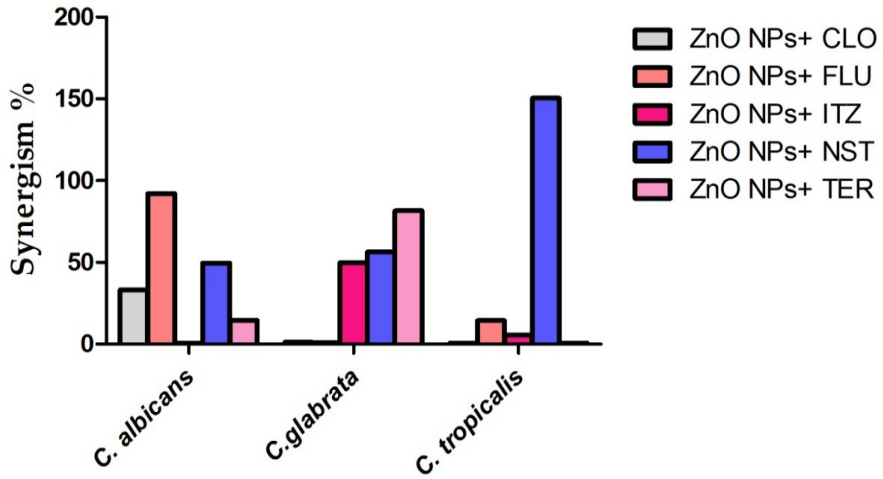

Figure 11. Synergistic percentages of green synthesized zinc oxide nanoparticles with different antifungal agents.

Table 3. Antifungal efficiency of the biogenic ZnO NPs compared to different antifungal agents.

Concentrations (µg/Disk)	Inhibition Zone Diameter (mm)					
	Candida albicans	*Candida glabrata*	*Candida tropicalis*	S	I	R
CLO (10 µg)	16.34 ± 0.26 (I)	25.45 ± 0.34 (S)	32.45 ± 0.27 (S)	≥20	12–19	<11
CLO (10 µg) + ZnO NPs (10 µg)	21.78 ± 0.17	25.78 ± 0.13	31.56 ± 0.18			
FLU (25 µg)	8.79 ± 0.12 (R)	24.34 ± 0.13 (S)	30.12 ± 0.25 (S)	≥22	15–21	<14
FLU (25 µg) + ZnO NPs (10 µg)	16.89 ± 0.29	24.57 ± 0.24	34.45 ± 0.31			
ITZ (10 µg)	20.78 ± 0.42 (I)	12.23 ± 0.41 (R)	24.32 ± 0.14 (S)	≥23	14–22	<13
ITZ (10 µg) + ZnO NPs (10 µg)	21.43 ± 019	18.34 ± 0.17	25.78 ± 0.19			
NST (25 µg)	15.67 ± 0.23 (S)	9.45 ± 0.24 (R)	9.01 ± 0.34 (R)	≥15	10–19	<10
NST (25 µg) + ZnO NPs (10 µg)	23.45 ± 0.11	14.78 ± 0.16	22.56 ± 0.67			
TER (30 µg)	28.34 ± 0.31 (S)	10.89 ± 0.16 (R)	37.89 ± 0.36 (S)	≥20	12–19	<11
TER (30 µg) + ZnO NPs (10 µg)	32.45 ± 0.42	19.78 ± 0.12	37.12 ± 0.56			

The synergistic mode of action between the biogenic ZnO NPs and antifungal drugs, such as nystatin, fluconazole, terbinafine and itraconazole, could be attributed to the fact that antifungal agents and ZnO NPs have different cellular targets, resulting in a boost in antifungal efficiency [89]. Combination therapy aims to reduce toxicity by lowering the standard administrative doses of drugs and boosting the antifungal effectiveness of conventional antifungal drugs [90].

The interactions between the biosynthesized ZnO NPs and antifungal drugs are classified into three main types: synergism, indifferent and antagonism [91]. Synergism occurs when the combined action of both ZnO NPs and antifungal drugs is higher than the action of a single antifungal agent, indicating that both ZnO NPs and the antifungal drug are targeting different cellular components [92]. In this regard, the biosynthesized ZnO NPs revealed synergistic action with terbinafine, nystatin and itraconazole against *C. glabrata* as a multidrug-resistant fungal pathogen. Furthermore, synergistic antifungal activity was detected between the biosynthesized ZnO NPs and antifungal agents, such as fluconazole, nystatin and clotrimazole against *C. albicans* strain.

Combined antifungal action is deemed indifferent if there is no discernible difference between the treatments and antagonistic if the effect is smaller than that of a single treatment [93]. On the other hand, the combined action of the biogenic ZnO NPs and itraconazole antifungal drugs against *C. tropicalis* and *C. albicans* strains is considered indifferent, whereas synergistic antifungal activity was detected between ZnO NPs and itraconazole against *C. glabrata*. Antagonistic antifungal action was detected between ZnO NPs and both clotrimazole and terbinafine against *C. tropicalis*. Collectively, the synergistic antifungal activity between the biogenic ZnO NPs and the tested antifungal agents highlights the potential of bioformulation of novel antifungal combinations to reduce the risk of acquiring antifungal resistance and lowering the toxicity of single-drug therapy [89].

The mechanism of antifungal activity of the biogenic ZnO NPs was reported previously in the literature as entering the fungal cell by diffusion and endocytosis, then interfering with the mitochondria in the cytoplasm, promoting the release of reactive oxygen species and Zn^{2+} ions [94]. These released Zn^{2+} ions passed through the fungal membrane and interacted with cellular DNA, causing nuclear damage, such as permanent chromosomal damage, and, finally, induction of cell death [95]. Previous studies reported that the antimicrobial efficiency of ZnO nanoparticles could be assigned to the generation of reactive oxygen species (ROS) [96]. Reactive oxygen species, such as hydrogen peroxide (H_2O_2), superoxide (O_2^-) and hydroxyl radical ($^{\cdot}OH$), prompt oxidative stress damage, resulting in disruption of cellular membranes, cellular proteins, nucleic acids and, finally, the induction of fungal cell death [97].

4. Conclusions

Punica granatum aqueous extract mediated green synthesis of ZnO NPs of potential physicochemical characteristics. The biosynthesized ZnO NPs revealed potential physicochemical characteristics, with an average particle size of 22.84 nm and a band gap energy of 3.4 eV. Furthermore, the biosynthesized ZnO NPs exhibited potent anticandidal efficiency against the tested fungal pathogens. The biosynthesized ZnO nanoparticles exhibited a potential synergistic efficiency with nystatin, terbinafine and itraconazole antifungal drugs against the multidrug-resistant strain *C. glabrata*. In this regard, the biogenic ZnO NPs synthesized using pomegranate peel extract could be a potential source of effective antifungal combinations against multidrug-resistant strains. Collectively, these findings highlight the potential of utilizing these ZnO nanomaterials in formulations of novel antifungal combinations with commonly used antifungal drugs to boost the antifungal efficiency of these agents and reduce the possible toxicities resulting from single antifungal agent administration.

Author Contributions: Conceptualization, M.T.Y. and A.A.A.-A.; methodology, M.T.Y.; software, M.T.Y.; validation, M.T.Y., A.A.A.-A. and F.O.A.-O.; formal analysis, A.A.A.-A., F.O.A.-O. and A.A.-F.M.; investigation, M.T.Y.; resources, A.A.A.-A.; data curation, M.T.Y.; writing—original draft preparation, M.T.Y.; writing—review and editing, M.T.Y., A.A.-F.M., A.A.A.-A. and F.O.A.-O.; visualization, A.A.-F.M.; supervision, A.A.A.-A. and F.O.A.-O.; project administration, A.A.A.-A.; funding acquisition, A.A.-F.M. All authors have read and agreed to the published version of the manuscript.

Funding: This study was funded by the Researchers Supporting Project (RSP-2021/362), King Saud University, Riyadh, Saudi Arabia.

Institutional Review Board Statement: Not applicable.

Informed Consent Statement: Not applicable.

Data Availability Statement: The datasets used and/or analyzed in the current study are available from the corresponding author upon reasonable request.

Acknowledgments: The authors extend their appreciation to the Researchers Supporting Project (RSP-2021/362), King Saud University, Riyadh, Saudi Arabia.

Conflicts of Interest: The authors declare no conflict of interest.

References

1. Ghazi, S.; Rafei, R.; Osman, M.; El Safadi, D.; Mallat, H.; Papon, N.; Dabboussi, F.; Bouchara, J.P.; Hamze, M. The epidemiology of Candida species in the Middle East and North Africa. *J. Mycol. Med.* **2019**, *29*, 245–252. [CrossRef] [PubMed]
2. Miceli, M.H.; Díaz, J.A.; Lee, S.A. Emerging opportunistic yeast infections. *Lancet Infect. Dis.* **2011**, *11*, 142–151. [CrossRef]
3. Costa-de-Oliveira, S.; Rodrigues, A.G. *Candida albicans* antifungal resistance and tolerance in bloodstream infections: The triad yeast-host-antifungal. *Microorganisms* **2020**, *8*, 154. [CrossRef] [PubMed]
4. Carolus, H.; Van Dyck, K.; Van Dijck, P. *Candida albicans* and Staphylococcus species: A threatening twosome. *Front. Microbiol.* **2019**, *10*, 2162. [CrossRef] [PubMed]
5. Lee, Y.; Puumala, E.; Robbins, N.; Cowen, L.E. Antifungal drug resistance: Molecular mechanisms in *Candida albicans* and beyond. *Chem. Rev.* **2020**, *121*, 3390–3411. [CrossRef] [PubMed]
6. Yassin, M.T.; Mostafa, A.A.; Al-Askar, A.A.; Bdeer, R. In vitro antifungal resistance profile of *Candida* strains isolated from Saudi women suffering from vulvovaginitis. *Eur. J. Med. Res.* **2020**, *25*, 1–9. [CrossRef]
7. Bayda, S.; Adeel, M.; Tuccinardi, T.; Cordani, M.; Rizzolio, F. The history of nanoscience and nanotechnology: From chemical–physical applications to nanomedicine. *Molecules* **2019**, *25*, 112. [CrossRef]
8. Puri, T.; Pathak, Y.; Parayil, G. Nanotechnology-Based Research Priorities for Global Sustainability. In *Sustainable Nanotechnology: Strategies, Products, and Applications*; John Wiley & Sons, Inc.: Hoboken, NJ, USA, 2022; pp. 1–15.
9. Ali, A.; Hira Zafar, M.Z.; ul Haq, I.; Phull, A.R.; Ali, J.S.; Hussain, A. Synthesis, characterization, applications, and challenges of iron oxide nanoparticles. *Nanotechnol. Sci. Appl.* **2016**, *9*, 49. [CrossRef]
10. Raghuwanshi, N.; Srivastava, A.K.; Yadav, T.C.; Gupta, S.; Khatri, K.; Pruthi, V.; Pruthi, V. Biogenic nanoparticles as theranostic agents: Prospects and challenges. In *Integrating Green Chemistry and Sustainable Engineering*; Scrivener Publishing LLC: Beverly, MA, USA, 2019; pp. 647–684.
11. Dontsova, T.A.; Nahirniak, S.V.; Astrelin, I.M. Metaloxide nanomaterials and nanocomposites of ecological purpose. *J. Nanomater.* **2019**, *2019*, 5942194. [CrossRef]
12. Iftikhara, M.M.I.; Azhara, I.; Sohaila, M.; Nadeema, Z.U.M.; Farooqia, R.; Ayuba, A.H.; Siddiquib, A.F.M.; ur Rehmana, Z.W. Sufficiency and toxicity limits of metallic oxide nanoparticles in the biosphere. *Nanomater. Synth. Charact. Hazards Saf.* **2021**, 145–192.
13. Mohd Yusof, H.; Mohamad, R.; Zaidan, U.H.; Rahman, A. Microbial synthesis of zinc oxide nanoparticles and their potential application as an antimicrobial agent and a feed supplement in animal industry: A review. *J. Anim. Sci. Biotechnol.* **2019**, *10*, 57. [CrossRef] [PubMed]
14. Carofiglio, M.; Barui, S.; Cauda, V.; Laurenti, M. Doped zinc oxide nanoparticles: Synthesis, characterization and potential use in nanomedicine. *Appl. Sci* **2020**, *10*, 5194. [CrossRef]
15. Li, Y.; Yang, Y.; Yun'an Qing, R.L.; Tang, X.; Guo, D.; Qin, Y. Enhancing ZnO-NP antibacterial and osteogenesis properties in orthopedic applications: A review. *Int. J. Nanomed.* **2020**, *15*, 6247. [CrossRef] [PubMed]
16. Chopra, H.; Bibi, S.; Singh, I.; Hasan, M.M.; Khan, M.S.; Yousafi, Q.; Baig, A.A.; Rahman, M.; Islam, F.; Emran, T.B.; et al. Green Metallic Nanoparticles: Biosynthesis to Applications. *Front. Bioeng. Biotechnol.* **2022**, *10*, 874742. [CrossRef] [PubMed]
17. Bandeira, M.; Giovanela, M.; Roesch-Ely, M.; Devine, D.M.; da Silva Crespo, J. Green synthesis of zinc oxide nanoparticles: A review of the synthesis methodology and mechanism of formation. *Sustain. Chem. Pharm.* **2020**, *15*, 100223. [CrossRef]
18. Kalpana, V.; Devi Rajeswari, V. A review on green synthesis, biomedical applications, and toxicity studies of ZnO NPs. *Bioinorg. Chem. Appl.* **2018**, *2018*, 3569758. [CrossRef]

19. Jeevanandam, J.; Kiew, S.F.; Boakye-Ansah, S.; Lau, S.Y.; Barhoum, A.; Danquah, M.K.; Rodrigues, J. Green approaches for the synthesis of metal and metal oxide nanoparticles using microbial and plant extracts. *Nanoscale* **2022**, *14*, 2534–2571. [CrossRef]
20. Majeed, M.I.; Bhatti, H.N.; Nawaz, H.; Kashif, M. Nanobiotechnology: Applications of nanomaterials in biological research. In *Integrating Green Chemistry and Sustainable Engineering*; Scrivener Publishing LLC: Beverly, MA, USA, 2019; pp. 581–615.
21. Król, A.; Railean-Plugaru, V.; Pomastowski, P.; Buszewski, B. Phytochemical investigation of *Medicago sativa* L. extract and its potential as a safe source for the synthesis of ZnO nanoparticles: The proposed mechanism of formation and antimicrobial activity. *Phytochem. Lett.* **2019**, *31*, 170–180. [CrossRef]
22. Dutta, G.; Sugumaran, A. Bioengineered zinc oxide nanoparticles: Chemical, green, biological fabrication methods and its potential biomedical applications. *J. Drug Deliv. Sci. Technol.* **2021**, *66*, 102853. [CrossRef]
23. Jafarirad, S.; Mehrabi, M.; Divband, B.; Kosari-Nasab, M. Biofabrication of zinc oxide nanoparticles using fruit extract of *Rosa canina* and their toxic potential against bacteria: A mechanistic approach. *Mater. Sci. Eng. C* **2016**, *59*, 296–302. [CrossRef]
24. Happy, A.; Soumya, M.; Kumar, S.V.; Rajeshkumar, S.; Sheba, R.D.; Lakshmi, T.; Nallaswamy, V.D. Phyto-assisted synthesis of zinc oxide nanoparticles using *Cassia alata* and its antibacterial activity against *Escherichia coli*. *Biochem. Biophys. Rep.* **2019**, *17*, 208–211. [CrossRef] [PubMed]
25. Jose, A.; Devi, K.S.; Pinheiro, D.; Narayana, S.L. Electrochemical synthesis, photodegradation and antibacterial properties of PEG capped zinc oxide nanoparticles. *J. Photochem. Photobiol. B Biol.* **2018**, *187*, 25–34. [CrossRef] [PubMed]
26. Pachaiappan, R.; Rajendran, S.; Ramalingam, G.; Vo, D.-V.N.; Priya, P.M.; Soto-Moscoso, M. Green synthesis of zinc oxide nanoparticles by Justicia adhatoda leaves and their antimicrobial activity. *Chem. Eng. Technol.* **2021**, *44*, 551–558. [CrossRef]
27. Nisar, P.; Ali, N.; Rahman, L.; Ali, M.; Shinwari, Z.K. Antimicrobial activities of biologically synthesized metal nanoparticles: An insight into the mechanism of action. *J. Biol. Inorg. Chem.* **2019**, *24*, 929–941. [CrossRef]
28. Pillai, A.M.; Sivasankarapillai, V.S.; Rahdar, A.; Joseph, J.; Sadeghfar, F.; Rajesh, K.; Kyzas, G.Z. Green synthesis and characterization of zinc oxide nanoparticles with antibacterial and antifungal activity. *J. Mol. Struct.* **2020**, *1211*, 128107. [CrossRef]
29. Hasaballah, A.I.; El-Naggar, H.A.; Abdelbary, S.; Bashar, M.A.; Selim, T.A. Eco-friendly Synthesis of Zinc Oxide Nanoparticles by Marine Sponge, Spongia officinalis: Antimicrobial and Insecticidal Activities Against the Mosquito Vectors, *Culex pipiens* and *Anopheles pharoensis*. *BioNanoScience* **2022**, *12*, 89–104. [CrossRef]
30. Zhu, W.; Hu, C.; Ren, Y.; Lu, Y.; Song, Y.; Ji, Y.; Han, C.; He, J. Green synthesis of zinc oxide nanoparticles using *Cinnamomum camphora* (L.) Presl leaf extracts and its antifungal activity. *J. Environ. Chem. Eng.* **2021**, *9*, 106659. [CrossRef]
31. Lingaraju, K.; Raja Naika, H.; Manjunath, K.; Basavaraj, R.; Nagabhushana, H.; Nagaraju, G.; Suresh, D. Biogenic synthesis of zinc oxide nanoparticles using *Ruta graveolens* (L.) and their antibacterial and antioxidant activities. *Appl. Nanosci.* **2016**, *6*, 703–710. [CrossRef]
32. Santhoshkumar, J.; Kumar, S.V.; Rajeshkumar, S. Synthesis of zinc oxide nanoparticles using plant leaf extract against urinary tract infection pathogen. *Resour.-Effic. Technol.* **2017**, *3*, 459–465. [CrossRef]
33. Yassin, M.T.; Mostafa, A.A.-F.; Al Askar, A.A. In Vitro Evaluation of Biological Activities and Phytochemical Analysis of Different Solvent Extracts of *Punica granatum* L. (Pomegranate) Peels. *Plants* **2021**, *10*, 2742. [CrossRef]
34. Singh, M.; Lee, K.E.; Vinayagam, R.; Kang, S.G. Antioxidant and Antibacterial Profiling of Pomegranate-pericarp Extract Functionalized-zinc Oxide Nanocomposite. *Biotechnol. Bioprocess Eng.* **2021**, *26*, 728–737. [CrossRef] [PubMed]
35. Ifeanyichukwu, U.L.; Fayemi, O.E.; Ateba, C.N. Green synthesis of zinc oxide nanoparticles from pomegranate (*Punica granatum*) extracts and characterization of their antibacterial activity. *Molecules* **2020**, *25*, 4521. [CrossRef] [PubMed]
36. Abdelmigid, H.M.; Hussien, N.A.; Alyamani, A.A.; Morsi, M.M.; AlSufyani, N.M.; Kadi, H.A. Green Synthesis of Zinc Oxide Nanoparticles Using Pomegranate Fruit Peel and Solid Coffee Grounds vs. Chemical Method of Synthesis, with Their Biocompatibility and Antibacterial Properties Investigation. *Molecules* **2022**, *27*, 1236. [CrossRef] [PubMed]
37. Yassin, M.T.; Mostafa, A.A.F.; Al-Askar, A.A.; Al-Otibi, F.O. Facile Green Synthesis of Silver Nanoparticles Using Aqueous Leaf Extract of *Origanum majorana* with Potential Bioactivity against Multidrug Resistant Bacterial Strains. *Crystals* **2022**, *12*, 603. [CrossRef]
38. He, G.; Huang, B.; Lin, Z.; Yang, W.; He, Q.; Li, L. Morphology transition of ZnO nanorod arrays synthesized by a two-step aqueous solution method. *Crystals* **2018**, *8*, 152. [CrossRef]
39. Priyadharshini, S.S.; Shubha, J.P.; Shivalingappa, J.; Adil, S.F.; Kuniyil, M.; Hatshan, M.R.; Shaik, B.; Kavalli, K. Photocatalytic Degradation of Methylene Blue and Metanil Yellow Dyes Using Green Synthesized Zinc Oxide (ZnO) Nanocrystals. *Crystals* **2021**, *12*, 22. [CrossRef]
40. Alharthi, F.A.; Alghamdi, A.A.; Alothman, A.A.; Almarhoon, Z.M.; Alsulaiman, M.F.; Al-Zaqri, N. Green synthesis of ZnO nanostructures using *Salvadora Persica* leaf extract: Applications for photocatalytic degradation of methylene blue dye. *Crystals* **2020**, *10*, 441. [CrossRef]
41. CLSI. *Method for Antifungal Disk Diffusion Susceptibility Testing of Yeasts*; CLSI m44-a, 23; Clinical and Laboratory Standards Institute: Wayne, PA, USA, 2004.
42. CLSI. *Performance Standards for Antifungal Susceptibility Testing of Yeasts*, 1st ed.; CLSI Suppl m60; Clinical and Laboratory Standards Institute: Wayne, PA, USA, 2017.
43. Yassin, M.T.; Mostafa, A.A.F.; Al-Askar, A.A. In vitro anticandidal potency of *Syzygium aromaticum* (clove) extracts against vaginal candidiasis. *BMC Complement. Altern. Med.* **2020**, *20*, 25. [CrossRef]

44. Singh, R.; Wagh, P.; Wadhwani, S.; Gaidhani, S.; Kumbhar, A.; Bellare, J.; Chopade, B.A. Synthesis, optimization, and characterization of silver nanoparticles from *Acinetobacter calcoaceticus* and their enhanced antibacterial activity when combined with antibiotics. *Int. J. Nanomed.* **2013**, *8*, 4277.
45. Huang, W.; Yan, M.; Duan, H.; Bi, Y.; Cheng, X.; Yu, H. Synergistic antifungal activity of green synthesized silver nanoparticles and epoxiconazole against *Setosphaeria turcica*. *J. Nanomater.* **2020**, *2020*, 9535432. [CrossRef]
46. Lo, W.H.; Deng, F.S.; Chang, C.J.; Lin, C.H. Synergistic antifungal activity of chitosan with fluconazole against *Candida albicans*, *Candida tropicalis*, and fluconazole-resistant strains. *Molecules* **2020**, *25*, 5114. [CrossRef] [PubMed]
47. Moteriya, P.; Padalia, H.; Chanda, S. Characterization, synergistic antibacterial and free radical scavenging efficacy of silver nanoparticles synthesized using *Cassia roxburghii* leaf extract. *J. Genet. Eng. Biotechnol.* **2017**, *15*, 505–513. [CrossRef] [PubMed]
48. Singh, B.; Singh, J.P.; Kaur, A.; Singh, N. Phenolic compounds as beneficial phytochemicals in pomegranate (*Punica granatum* L.) peel: A review. *Food Chem.* **2018**, *261*, 75–86. [CrossRef] [PubMed]
49. Sukri, S.N.A.M.; Shameli, K.; Wong, M.M.T.; Teow, S.Y.; Chew, J.; Ismail, N.A. Cytotoxicity and antibacterial activities of plant-mediated synthesized zinc oxide (ZnO) nanoparticles using *Punica granatum* (pomegranate) fruit peels extract. *J. Mol. Struct.* **2019**, *1189*, 57–65. [CrossRef]
50. Fuku, X.; Diallo, A.; Maaza, M. Nanoscaled electrocatalytic optically modulated ZnO nanoparticles through green process of *Punica granatum* L. and their antibacterial activities. *Int. J. Electrochem. Sci.* **2016**, *2016*, 4682967.
51. Singh, K.; Singh, J.; Rawat, M. Green synthesis of zinc oxide nanoparticles using *Punica Granatum* leaf extract and its application towards photocatalytic degradation of Coomassie brilliant blue R-250 dye. *SN Appl. Sci.* **2019**, *1*, 624. [CrossRef]
52. Siva, N.; Sakthi, D.; Ragupathy, S.; Arun, V.; Kannadasan, N. Synthesis, structural, optical and photocatalytic behavior of Sn doped ZnO nanoparticles. *Mater. Sci. Eng. B* **2020**, *253*, 114497. [CrossRef]
53. Jan, F.A.; Ullah, R.; Ullah, N.; Usman, M. Exploring the environmental and potential therapeutic applications of *Myrtus communis* L. assisted synthesized zinc oxide (ZnO) and iron doped zinc oxide (Fe-ZnO) nanoparticles. *J. Saudi Chem. Soc.* **2021**, *25*, 101278.
54. Ramesh, M.; Anbuvannan, M.; Viruthagiri, G. Green synthesis of ZnO nanoparticles using *Solanum nigrum* leaf extract and their antibacterial activity. *Spectrochim. Acta A Mol. Biomol. Spectrosc.* **2015**, *136*, 864–870. [CrossRef]
55. Rathore, R.; Kaurav, N. The structural and optical properties of ZnO nanoparticles synthesized via thermal decomposition. *Mater. Today Proc.* **2022**, *54*, 624–627. [CrossRef]
56. Babitha, N.; Priya, L.S.; Christy, S.R.; Manikandan, A.; Dinesh, A.; Durka, M.; Arunadevi, S. Enhanced antibacterial activity and photo-catalytic properties of ZnO nanoparticles: *Pedalium murex* plant extract-assisted synthesis. *J. Nanosci. Nanotechnol.* **2019**, *19*, 2888–2894. [CrossRef] [PubMed]
57. Kumar, V.; Gohain, M.; Kant, R.; Ntwaeaborwa, O.M.; Hari, P.; Swart, H.C.; Dutta, V. Annealing induced oxygen defects on green sonochemically synthesized ZnO nanoparticles for photoelectrochemical water splitting. *ChemistrySelect* **2018**, *3*, 11914–11921. [CrossRef]
58. Barani, M.; Masoudi, M.; Mashreghi, M.; Makhdoumi, A.; Eshghi, H. Cell-free extract assisted synthesis of ZnO nanoparticles using aquatic bacterial strains: Biological activities and toxicological evaluation. *Int. J. Pharm.* **2021**, *606*, 120878. [CrossRef] [PubMed]
59. Motaung, D.E.; Mhlongo, G.H.; Nkosi, S.S.; Malgas, G.F.; Mwakikunga, B.W.; Coetsee, E.; Swart, H.C.; Abdallah, H.M.; Moyo, T.; Ray, S.S. Shape-selective dependence of room temperature ferromagnetism induced by hierarchical ZnO nanostructures. *ACS Appl. Mater. Interfaces* **2014**, *6*, 8981–8995. [CrossRef]
60. Vimala, K.; Sundarraj, S.; Paulpandi, M.; Vengatesan, S.; Kannan, S. Green synthesized doxorubicin loaded zinc oxide nanoparticles regulates the Bax and Bcl-2 expression in breast and colon carcinoma. *Process Biochem.* **2014**, *49*, 160–172. [CrossRef]
61. Nagalingam, M.; Rajeshkumar, S.; Balu, S.K.; Tharani, M.; Arunachalam, K. Anticancer and Antioxidant Activity of *Morinda Citrifolia* Leaf Mediated Selenium Nanoparticles. *J. Nanomater.* **2022**, *2022*, 2155772. [CrossRef]
62. Rao, K.J.; Paria, S. Green synthesis of silver nanoparticles from aqueous Aegle marmelos leaf extract. *Mater. Res. Bull.* **2013**, *48*, 628–634.
63. Selvarajan, E.; Mohanasrinivasan, V. Biosynthesis and characterization of ZnO nanoparticles using *Lactobacillus plantarum* VITES07. *Mater. Lett.* **2013**, *112*, 180–182. [CrossRef]
64. Vijayakumar, S.; Vaseeharan, B.; Malaikozhundan, B.; Divya, M.; Abhinaya, M.; Gobi, N.; Bhattacharyya, A.; Balashanmugam, N.; Surmistha, D.; Murugan, K.; et al. Ecotoxicity of *Musa paradisiaca* leaf extract-coated ZnO nanoparticles to the freshwater microcrustacean *Ceriodaphnia cornuta*. *Limnologica* **2017**, *67*, 1–6. [CrossRef]
65. Chung, I.M.; Rahuman, A.A.; Marimuthu, S.; Kirthi, A.V.; Anbarasan, K.; Rajakumar, G. An investigation of the cytotoxicity and caspase-mediated apoptotic effect of green synthesized zinc oxide nanoparticles using *Eclipta prostrata* on human liver carcinoma cells. *Nanomaterials* **2015**, *5*, 1317–1330. [CrossRef]
66. Ravichandran, V.; Sumitha, S.; Ning, C.Y.; Xian, O.Y.; Kiew Yu, U.; Paliwal, N.; Shah, S.A.A.; Tripathy, M. Durian waste mediated green synthesis of zinc oxide nanoparticles and evaluation of their antibacterial, antioxidant, cytotoxicity and photocatalytic activity. *Green Chem. Lett. Rev.* **2020**, *13*, 102–116. [CrossRef]
67. Vijayakumar, S.; Mahadevan, S.; Arulmozhi, P.; Sriram, S.; Praseetha, P.K. Green synthesis of zinc oxide nanoparticles using *Atalantia monophylla* leaf extracts: Characterization and antimicrobial analysis. *Mat. Sci. Semicond. Proc.* **2018**, *82*, 39–45. [CrossRef]

68. Ezealisiji, K.M.; Siwe-Noundou, X.; Maduelosi, B.; Nwachukwu, N.; Krause, R.W.M. Green synthesis of zinc oxide nanoparticles using *Solanum torvum* (L) leaf extract and evaluation of the toxicological profile of the ZnO nanoparticles–hydrogel composite in Wistar albino rats. *Int. Nano Lett.* **2019**, *9*, 99–107. [CrossRef]
69. Sattari, R.; Khayati, G.R.; Hoshyar, R. Biosynthesis and characterization of silver nanoparticles capped by biomolecules by *fumaria parviflora* extract as green approach and evaluation of their cytotoxicity against human breast cancer MDA-MB-468 cell lines. *Mater. Chem. Phys.* **2020**, *241*, 122438. [CrossRef]
70. Faisal, S.; Jan, H.; Shah, S.A.; Shah, S.; Khan, A.; Akbar, M.T.; Rizwan, M.; Jan, F.; Wajidullah; Akhtar, N.; et al. Green synthesis of zinc oxide (ZnO) nanoparticles using aqueous fruit extracts of *Myristica fragrans*: Their characterizations and biological and environmental applications. *ACS Omega* **2021**, *6*, 9709–9722. [CrossRef] [PubMed]
71. Barzinjy, A.A.; Azeez, H.H. Green synthesis and characterization of zinc oxide nanoparticles using *Eucalyptus globulus* Labill. leaf extract and zinc nitrate hexahydrate salt. *SN Appl. Sci.* **2020**, *2*, 991. [CrossRef]
72. Al-Kordy, H.M.; Sabry, S.A.; Mabrouk, M.E. Statistical optimization of experimental parameters for extracellular synthesis of zinc oxide nanoparticles by a novel haloalaliphilic *Alkalibacillus* sp.W7. *Sci. Rep.* **2021**, *11*, 10924. [CrossRef]
73. Abomuti, M.A.; Danish, E.Y.; Firoz, A.; Hasan, N.; Malik, M.A. Green Synthesis of Zinc Oxide Nanoparticles Using *Salvia officinalis* Leaf Extract and Their Photocatalytic and Antifungal Activities. *Biology* **2021**, *10*, 1075. [CrossRef]
74. Negi, A.; Gangwar, R.; Vishwakarma, R.K.; Negi, D.S. Biogenic zinc oxide nanoparticles as an antibacterial, antifungal, and photocatalytic tool mediated via leaves of *Girardinia diversifolia*. *Nanotechnol. Environ. Eng.* **2022**, *7*, 223–233. [CrossRef]
75. Miri, A.; Mahdinejad, N.; Ebrahimy, O.; Khatami, M.; Sarani, M. Zinc oxide nanoparticles: Biosynthesis, characterization, antifungal and cytotoxic activity. *Mater. Sci. Eng. C* **2019**, *104*, 109981. [CrossRef]
76. Spampinato, C.; Leonardi, D. Candida infections, causes, targets, and resistance mechanisms: Traditional and alternative antifungal agents. *Biomed. Res. Int.* **2013**, *2013*, 204237. [CrossRef] [PubMed]
77. Pristov, K.E.; Ghannoum, M.A. Resistance of *Candida* to azoles and echinocandins worldwide. *Clin. Microbiol. Infect.* **2019**, *25*, 792–798. [CrossRef] [PubMed]
78. Krishnasamy, L.; Krishnakumar, S.; Kumaramanickavel, G.; Saikumar, C. Molecular mechanisms of antifungal drug resistance in Candida species. *J. Clin. Diagnostic Res.* **2018**, *12*, DE01–DE06. [CrossRef]
79. Shi, Y.; Zhu, Y.; Fan, S.; Liu, X.; Liang, Y.; Shan, Y. Molecular identification and antifungal susceptibility profile of yeast from vulvovaginal candidiasis. *BMC Infect. Dis.* **2020**, *20*, 287. [CrossRef]
80. Jayachandran, A.L.; Katragadda, R.; Thyagarajan, R.; Vajravelu, L.; Manikesi, S.; Kaliappan, S.; Jayachandran, B. Oral Candidiasis among cancer patients attending a tertiary Care Hospital in Chennai, South India: An evaluation of Clinicomycological association and antifungal susceptibility pattern. *Can. J. Infect. Dis. Med. Microbiol.* **2016**, *2016*, 8758461. [CrossRef]
81. Bhattacharya, S.; Sae-Tia, S.; Fries, B.C. Candidiasis and mechanisms of antifungal resistance. *Antibiotics* **2020**, *9*, 312. [CrossRef]
82. Quindós, G.; Gil-Alonso, S.; Marcos-Arias, C.; Sevillano, E.; Mateo, E.; Jauregizar, N.; Eraso, E. Therapeutic tools for oral candidiasis: Current and new antifungal drugs. *Med. Oral Patol. Oral Cir. Bucal* **2019**, *24*, e172. [CrossRef]
83. Carolus, H.; Pierson, S.; Lagrou, K.; Van Dijck, P. Amphotericin B and other polyenes—Discovery, clinical use, mode of action and drug resistance. *J. Fungi* **2020**, *6*, 321. [CrossRef]
84. Esfahani, A.N.; Golestannejad, Z.; Khozeimeh, F.; Dehghan, P.; Maheronnaghsh, M.; Zarei, Z. Antifungal effect of Atorvastatin against Candida species in comparison to Fluconazole and Nystatin. *Med. Pharm. Rep.* **2019**, *92*, 368. [CrossRef]
85. Ahmed, M.Z.; Rao, T.; Saeed, A.; Mutahir, Z.; Hameed, S.; Inayat, S.; Shahzad, H.; Ullah, N.; Abaid-Ullah, M.; Ibrahim, M.; et al. Antifungal Drugs: Mechanism of Action and Resistance. In *Biochemistry of Drug Resistance*; Springer: Cham, Switzerland, 2021; pp. 143–165.
86. Ivanov, M.; Ćirić, A.; Stojković, D. Emerging Antifungal Targets and Strategies. *Int. J. Mol. Sci.* **2022**, *23*, 2756. [CrossRef]
87. Fatahinia, M.; Halvaeizadeh, M.; Mahmoudabadi, A.Z.; AboualiGalehdari, E.; Kiasat, N. In vitro antifungal susceptibilities of six antifungal drugs against clinical *Candida glabrata* isolates according to EUCAST. *Curr. Med. Mycol.* **2020**, *6*, 1–6. [CrossRef] [PubMed]
88. Sacheli, R.; Hayette, M.P. Antifungal Resistance in Dermatophytes: Genetic Considerations, Clinical Presentations and Alternative Therapies. *J. Fungi* **2021**, *7*, 983. [CrossRef] [PubMed]
89. Chand, P.; Kumari, S.; Mondal, N.; Singh, S.P.; Prasad, T. Synergism of Zinc Oxide Quantum Dots with Antifungal Drugs: Potential Approach for Combination Therapy against Drug Resistant *Candida albicans*. *Front. Nanotech.* **2021**, *3*, 32. [CrossRef]
90. Scorzoni, L.; Sangalli-Leite, F.; de Lacorte Singulani, J.; Costa-Orlandi, C.B.; Fusco-Almeida, A.M.; Mendes-Giannini, M.J.S. Searching new antifungals: The use of in vitro and in vivo methods for evaluation of natural compounds. *J. Microbiol. Methods* **2016**, *123*, 68–78. [CrossRef]
91. Brescini, L.; Fioriti, S.; Morroni, G.; Barchiesi, F. Antifungal combinations in dermatophytes. *J. Fungi* **2021**, *7*, 727. [CrossRef]
92. Sun, Q.; Li, J.; Le, T. Zinc oxide nanoparticle as a novel class of antifungal agents: Current advances and future perspectives. *J. Agric. Food Chem.* **2018**, *66*, 11209–11220. [CrossRef]
93. Saracino, I.M.; Foschi, C.; Pavoni, M.; Spigarelli, R.; Valerii, M.C.; Spisni, E. Antifungal Activity of Natural Compounds vs. *Candida* spp.: A Mixture of Cinnamaldehyde and Eugenol Shows Promising In Vitro Results. *Antibiotics* **2022**, *11*, 73. [CrossRef]
94. Agarwal, H.; Rajeshkumar, S.; Shanmugam, V.K. Microbe-mediated synthesis of zinc oxide nanoparticles. In *Zinc-Based Nanostructures for Environmental and Agricultural Applications*; Elsevier: Amsterdam, The Netherlands, 2021; pp. 53–63.

95. Patra, P.; Mitra, S.; Debnath, N.; Goswami, A. Biochemical-, biophysical-, and microarray-based antifungal evaluation of the buffer-mediated synthesized nano zinc oxide: An in vivo and in vitro toxicity study. *Langmuir* **2012**, *28*, 16966–16978. [CrossRef]
96. Lipovsky, A.; Nitzan, Y.; Gedanken, A.; Lubart, R. Antifungal activity of ZnO nanoparticles—The role of ROS mediated cell injury. *Nanotechnology* **2011**, *22*, 105101. [CrossRef]
97. Sharma, S.; Singh, V.K.; Kumar, A.; Mallubhotla, S. Effect of nanoparticles on oxidative damage and antioxidant defense system in plants. In *Molecular Plant Abiotic Stress: Biology and Biotechnology*; John Wiley & Sons, Ltd.: Hoboken, NJ, USA, 2019; pp. 315–333.